Design Journal Summary
FEEG6013 Group Design Project

45
Tesla Turbine Design

ID Number: 29070651
Name: Kai Jie Chow

1. Summary of Individual Contribution

Working as the team's numerical modeller, my task was to design, construct and analyse the flow physics established in our turbine prototype. Most of my work revolved about choosing and coding an appropriate mathematical model such that it closely represents that in practical settings. This was done under the incentive of pacing up simulation cases for quick design optimisation via simpler yet accurate model.

Via Python simulation tools, I formulated an entire analytical model, as well as performing the necessary design optimisation in view of manufacturing feasibility and desired engineering performances. In conjunction to that, I worked closely with the design team, coordinating and reiterating design selection based on results obtained. This selected design point will then be pushed into CFD analysis at which I played the part of bridging the process, giving detailed modelling and fluid mechanics insights for subsequent improvements. Furthermore, I also took part in the CFD result extrapolation phase, comparing and validating results with that extracted from the numerical set.

Additionally, I was also in charge of managing the project's embedded system programming for processing sensors' data. The platform for this has been constructed but was not put into actual practice due to restricted lab access and thus, design prototype not being manufactured.

2. Roles, Activities and Outputs

This section outlines my work progression starting with literature review/objectives, leading into tasks breakdown and lastly, the contribution of my role to the overall project flow.

2.1 Literature Review and Goals

In the Tesla Turbine, the principal mechanism for power generation occurs at the disc stack where fluid rotates the discs through adhesive effects. Due to its importance, there have been many studies done to characterise the flow within the disc stack as to better understand the influence of disc parameters and hence optimise its design.

With the objective of peak efficiency, numerical flow analysis was included in this study to capture key design factors impacting the turbine's flow. Working as the team's numerical modeller, I took charge in this by reviewing past literatures and studies regarding this topic (Design Journal 1). One of the earliest numerical investigations working on this front was published in 1965 by Warren Rice [1]. In their study, a crude analytical idealisation was devised such that it captured the flow profile with relative accuracy without requiring heavy mathematical complexity. Rice's methodology has since been attracting much attention in the field of Tesla Turbine analysis due to its simplicity and range of applicability. Following up on this, Sengupta et al. investigated a formulation for the inter-disc flow field in a three-dimensional setting under a fixed pressure drop [2]. Aside from the observed decreasing efficiency trend with higher flow rate, it was also noted that the experimental efficiencies were consistently lower than their analytical counterpart due to the omission of losses from bearings, nozzles and seals.

Similarly, Romanin and Carey developed a three-dimensional integral perturbation model with a surface micro-structuring incorporation, generalising upon the conventional Poiseuille flow assumption [3]. Dimensionless parameters were highlighted throughout the study to provide a direct assessment of their relative impacts on fluid pressure, viscosity and momentum. All of which ultimately affected turbine performance. In addition to Carey's work, Krishnan et al. applied a similar model with the inclusion of parameter-scaling and loss mechanisms as to practically correlate theoretical efficiency and thus design optimisation [4]. It was shown that the turbine was able to draw out near 40% efficiency when scaled down to the millimetre regime for incompressible flow (water).

Having reviewed multiple variants, I have chosen Carey and Romanin's version as the base reference. This is because the model encompasses a wide range of cases (better generality), surface microstructuring analysis as well as thorough results validation with that of experimental datasets, showing its suitability to predict turbine's performance index.

Numerical Modelling Aims:
To construct a comprehensive numerical model for turbine optimisation based on discs flow analysis under varying design parameters.
Objectives:
- Flow model construction for characterising flow between two rotating discs and its impacts on power generation.
- Model augmentations accounting for additional design aspects.
- Optimal design point and operating condition selection.
- Turbine scaling analysis and its effects on power density.
- Results validation with that obtained from CFD simulations and past research work.

2.2 Numerical Model
The main analytical treatment begins by considering flow delivered from the volute casing into the rotating discs. The Navier-Stokes equation was then modified based on assumptions postulated by previous research studies:

1) Steady, incompressible laminar flow solutions throughout.
2) Trivial flow velocity in axial direction (2D solutions).
3) The flow field was considered as azimuthally symmetric and thus, solutions are invariant in that direction.
4) Negligible entrance effects, i.e. fully constructed boundary layer.
5) Negligible body forces.

From the above idealisations, the governing equations can be reformulated and transformed as demonstrated in the Group Report (**Equations 1 - 25**). In essence, the full 3D Navier-Stokes equations can be summarised by the following ODEs, where solutions to these two equations provide a complete characterisation of the flow within the turbine.
Tangential ODE

$$-\frac{2n+1}{n+1} = \left[\frac{1}{\xi} - \frac{8(2n+1)\xi}{\mathrm{Re}_m^*}\right]\widehat{W} + \frac{\partial\widehat{W}}{\partial\xi} \tag{1}$$

Radial ODE

$$\frac{\partial\widehat{P}}{\partial\xi} = \frac{4(n+1)}{(2n+1)\xi^3}\left[V_{r0}{}^2 + \xi^2\widehat{W}^2\right] + 4\widehat{W} + 2\xi + \left(\frac{32(n+1)V_{r0}^2}{\mathrm{Re}_m^*\xi}\right) \tag{2}$$

Through these set of equations, I coded out a model with adjustable settings to extract performance data such as power generation (**Equation 27**), turbine mechanical (**Equation 28**) and ideal efficiency (**Equation 29**). Additionally, I respecified/converted several terms into engineering comprehensible expressions as to replicate setups such as that in practical settings.

Since most calculations would involve many variables, I have set a flowParameters class which consists of rotor discs specifications, disc RPM, mass flow rates and so on, essentially defining the whole turbine design aspect. Such means was specifically chosen not just due to better user readability, but also simplifying functional codes through instantiating design points, allowing quicker variables search and pinpointing. To solve the above ODEs, I first define an array of radial positions using **Numpy**, then applied a **Scipy Odeint** solver to solve the coupled set of ODEs through these discrete radial points. The final output will comprise of two columns worth of data, corresponding to the two ODEs' solution respectively. Subsequently, these two solutions can be applied to calculate torque, power, efficiency and many other performance related results. Every obtained result was displayed in graphical format using Matplotlib library, with different plot configurations that can best represent the data points. Moving on from here, I first plotted out diagrams to validate the model results with that from the literature, then I incorporated additional design formulation to the code before running case simulations. Through the case simulations plots, I can choose an optimal design point basing on turbine performance and manufacturing feasibility, which will ultimately be relayed over to CAD modelling for this project. Additionally, I also used these tools to perform extra analysis that can be useful for future analysis or design plan.

2.3 Volute Casing Modifications and Performance Optimisation
For our project's design, a volute casing was integrated with the rotor disc stacks, where flow will first progress and accelerate through the volute channel before entering the disc stacks (cross sectional design in **Figure 1**). As opposed to nozzle, which was widely implemented across the literature, volute casing provides the medium a spiralling pattern such that fluid's velocity can be more uniformly distributed throughout the discs' perimeter. Aside from that, the design simplicity also makes it much appealing for a huge range of applications.

Flow Angle and Boundary Conditions
It is rather apparent from **Figure 1** that under a fixed mass flow rate, the flow medium exits the volute casing at a certain speed and angle.
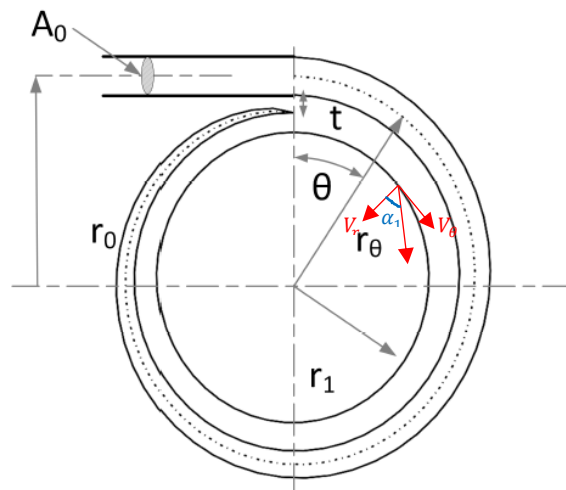
Figure 1 Volute casing cross section.

Applying angular momentum and mass conservation, the following relationship exists for exit flow angle [5],

$$tan(\alpha_1) = \frac{(A_1/r_1)}{(A_0/r_0)}$$

Through this formula, flow angle at the tip of the discs can be determined and thus, attaining the radial and tangential components of the flow which constitute the ODE boundary conditions.

With the above design selection, my subsequent task was to extend the code functionalities as to incorporate the aforementioned flow mechanisms. Most of it involves the flowParameters class redefinition, including volute casing parameters and the angle formula class Methods. Some simplifications were also added as described in the Group Report (**Equation 34 - 38**).

Initial Design Outline

Once the numerical model was fully constructed, I then worked closely with the team's design lead, Frederick Wong on specifying turbine's dimensions and parameters for laying out a design's baseline, before proceeding to optimisations.

Figure 2 illustrates the turbine's mechanical efficiency contour as a function of modified Reynolds number, Re_m^* and relative inlet dimensionless tangential velocity, W_0 at different radius ratio (Design Journal 3), ξ. From the diagram, we can spot a rather consistent pattern whereby efficiency increases moderately with W_0, but significantly with reducing Re_m^*. From the dimensionless definition of these two variables, one can conclude that lower tip disc speed or greater tangential velocity component can contribute to efficiency gain. This is obvious with the fact that tesla turbine works on the basis of shear force, which is contributed by the difference between the fluid velocity and that of the rotating discs. However, reducing disc speed may not necessarily favour power output as power is the product of both torque generated and the rotating speed. Therefore, optimisation on this front was required and was done so in the subsequent analysis.
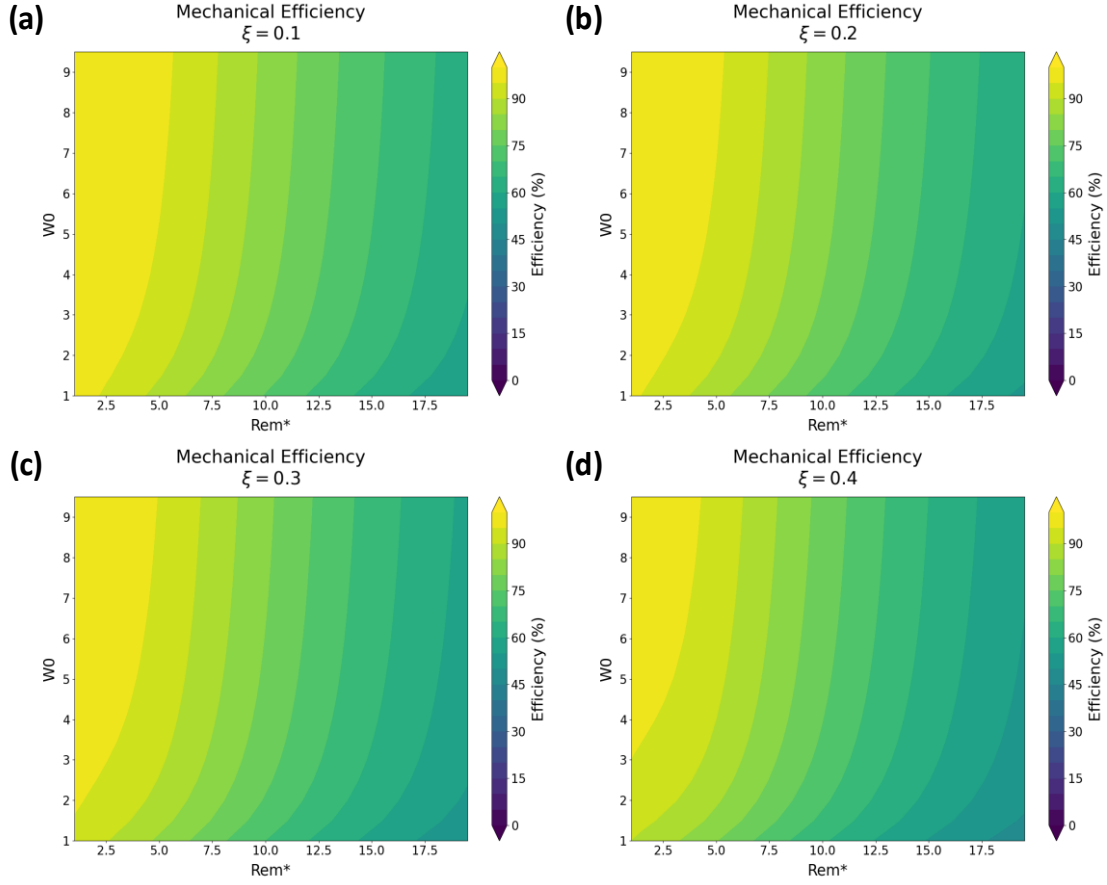
Figure 2 Mechanical Efficiency contour plots against Re_m^* and W_0 at V_{r0} = 0.05, with (a) 0.1, (b) 0.2, (c) 0.3 and (d) 0.4 radius ratio.

Aside from that, minimising inter-disc spacing can greatly improve turbine performance, due to its squared term dependence within Re_m^*. This result was well expected as smaller disc spacing give rise to higher fluid velocity per channel, increasing the near wall velocity gradient leading to higher shearing power. This reasoning was also supported by many literature studies as such, our team straight off implement the smallest manufacturable disc spacing which was set to 0.2mm.

Furthermore, the plots also imply that smaller radius ratio will generally give better turbine performance. At a fixed rotor outer radius, smaller ratio signifies greater surface exposure and thus, higher fluid momentum transfer to disc rotations. The above observation justifies our rotor radius dimensions, where we intend to maximise the ratio as much as possible. This however is limited by a few factors such as the imposed manufacturing limit which fixed the maximum outer radius; as well as choked flow occurrence which in turns restrained the minimum feasible inner radius. In this investigation, we have concluded that a fixed radius ratio of 0.3 would be a good balance between those two aspects to provide a good feasible range of manufacturable design simulations.

(a)   (b)
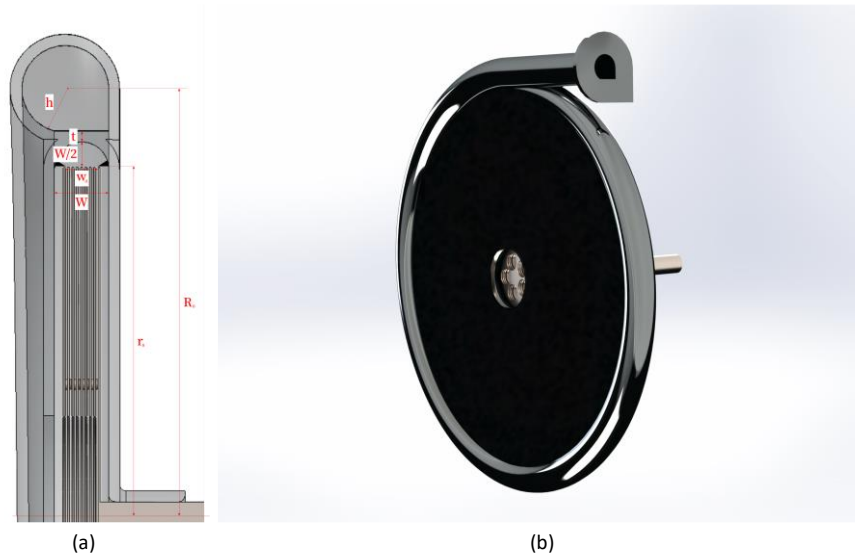
Figure 3 Cross sectional view and (b) Rendered Isometric view of the volute casing tesla turbine design.

*With all things considered, **Table 1** outlines the initial design parameters set for simulation purposes whereas **Figure 3** displays the turbine layout using SolidWorks. Mass flow rate was kept at 1kg/s which was well within the upper limit of allowable flow rate in university's laboratory settings.*

Table 1 Initial design parameters and values.

| Variables	Values
Mass Flow Rate, $\dot{m}$	1 kg/s
Volute Outer Radius, R_0	286 mm
Volute Inlet Radius, h	8.6 mm
Volute Thickness, t	5 mm
Disc Outer Radius, r_0	164 mm
Disc Inner Radius, r_i	49.2 mm
Radius Ratio, ξ_i	0.3
Inter-Disc Spacing, b	0.2 mm
Disc Thickness, t_d	0.8 mm
Disc Space, w_d	7.2 mm
Wall Clearance, w_c	1 mm
Disc Holder Width, W	10.8 mm
Disc Number, n_d	9
Flow Profile, n	2

Additionally, I also introduced several constraints, given by **Equations 34 - 38** in the Group Report, where these functions bind several variables together such as W, h and r_i. This was done to ensure the design's structural integrity remained well represented under scaling effects as well as limiting the number of free variables for simplifications.

From these relations, one can relate the entire design's measurements to just two fundamental variables, namely disc number, n_d and rotor disc outer radius, r_0. This approach was done intentionally as to simplify the simulation cases by capping the number of free variables, allowing full-on analysis without greatly sacrificing design flexibility.

Design Optimisation

As the group wanted to focus on turbine output, I then ran power simulations for different design by looping over a parametric sweep range of RPM, scaling factor and disc number

(Design Journal 4). **Figure *4*** illustrates the resulting power output contour from the mentioned simulation. Except for $n_d = 2$, the remaining plots appear to show consistent trends and conical structures, with slight variations in magnitude throughout. The exception applies because at $n_d = 2$, w_d will be relatively small and leads to a high turbine aspect ratio. According to **Equation 13**, this will result with an inlet angle that is more radial (near 40° from disc's tangent line). This greatly impacts the flow capability to transfer tangential shear momentum and thus, causing a significant difference in power output. As observed from the figure below, we can see that the power magnitude steadily increases till $n_d = 5$, before diminishing again as n_d continue to rise. Although the angle will be much favourable as n_d increases, but the flow velocity per channel reduces linearly with every subsequent addition due to mass conservation. Such occurrence implies that the tangential velocity component also reduces which then again, impacting the shear transfer and correspondingly, overall power output.
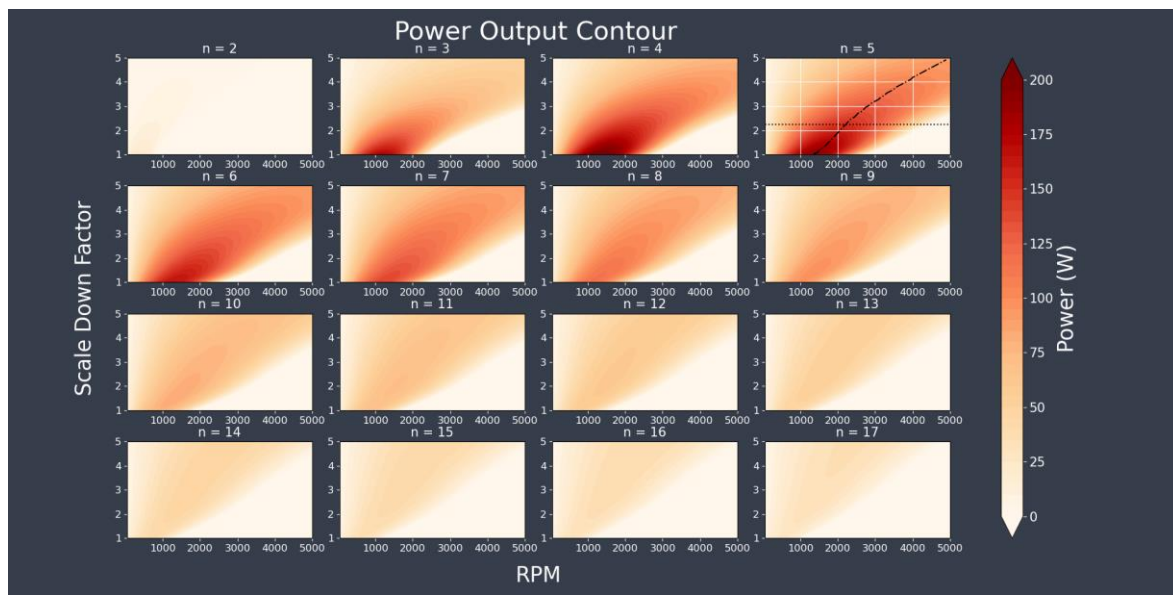
Figure 4 Power output contour at varying rpm and scale down factor across a range of disc numbers.

After careful inspection, I suggested a design point at $n_d = 5$, with a scale down factor of 2.25 as indicated by the horizontal line in the plot. Although all 16 plots show highest power output at scale factor of 1, but for manufacturing limitation reasons, this scale down factor was chosen so as to accommodate the aforementioned limitation. Moreover, at scale-down factor of 2.25, the plot also suggests a wide range of applicable RPM at which the turbine will be able to provide power output of more than 100W.

One other interesting observation spotted is the optimum RPM trend line variation with turbine dimensions. Combining with the scale down factor previously stated, the RPM of 2000 was selected for this study to which optimum performance can be expected.

2.3   Further Numerical Study

<u>**K-Exponent Scaling**</u>

Aside from optimising turbine design, I also did extra analysis on the scaling aspect to cover specifications which might be of relevance in future studies. In this investigation, a scale function such as the following formulation was derived to perform consecutive evaluations of scaling onto the turbine's overall performance.

$$b_{scale} = r_{scale}{}^k, \qquad 0 < k < 1$$

where b_{scale} and r_{scale} represent the inter-disc space and radial scaling factors, respectively.
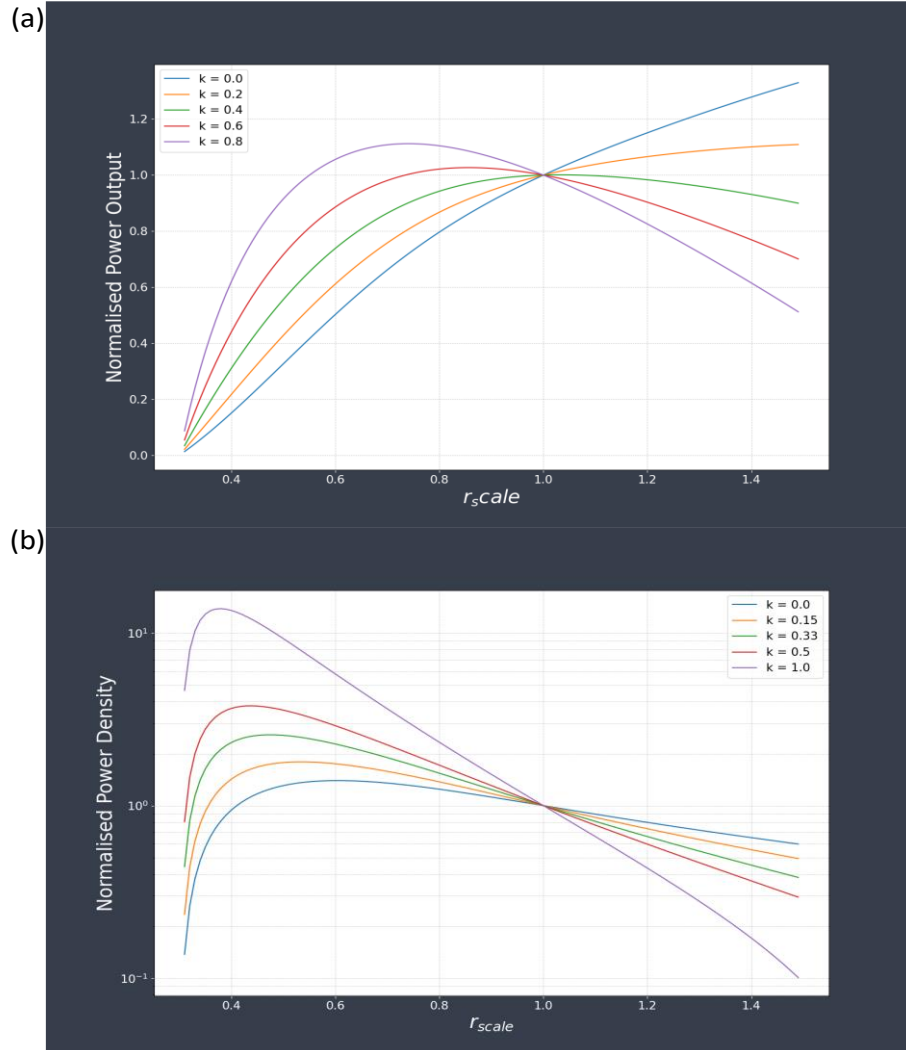

Figure 5 Graphs of (a) Normalised Power Output and (b) Normalised Power Density against Radial Scaling.

The plots in **Figure 5** provide the normalised turbine's power output and power density profiles under the scaling equation's effects. By setting the inner radius to a fixed value (22 mm) and RPM to 2000, I then proceeded on with the above scaling analysis via looping over an array of r_{scale} and k exponent. The results above do not just compare the turbine output performance, but also its density performance which can be associated with manufacturing cost. With these considered, the design choice selected in previous sections can still be justified as the most fitting and optimal point for this investigation.

Torque Analysis

The study so far has only considered cases where RPM can be freely configured. However, this is only true when implementing a variable load alternator whereas under common settings, that is hardly the case where torque is usually the fixed term, and RPM is allowed to change accordingly with the applied input force. In a tesla turbine, this force is directly extracted from the fluid's relative shear power to that of the rotating discs. Therefore, this inspired me to simulate cases under fixed torque and varying configurations. (*Note*: the following results were not included in the Group report due to space limitations)

Figure 6 shows the power contour plot similar to that in **Figure 4**, but with the x-axis adjusted to torque variable. This was done by using a root finding algorithm to back-track into the relevant RPM for a given specific torque and operating conditions. The results correspond well except that the trends seem to portray the inverse versions of that from the RPM counterpart. This is to be expected because at high RPM, the relative velocity difference will be smaller, essentially yielding lower torque values. It is also important to identify the 0-power region (upper right corner) of each plot, which signifies the maximum torque producible at any given scale down instance. From the diagram, we can conclude that on average, lower scale down factor designs are able to operate in a wider range of torque requirements; whereas the opposite is true at higher factor cases. In conjunction to that, with the current design point, the range of applicable torque lies between $0 - \sim1.2 Nm$.
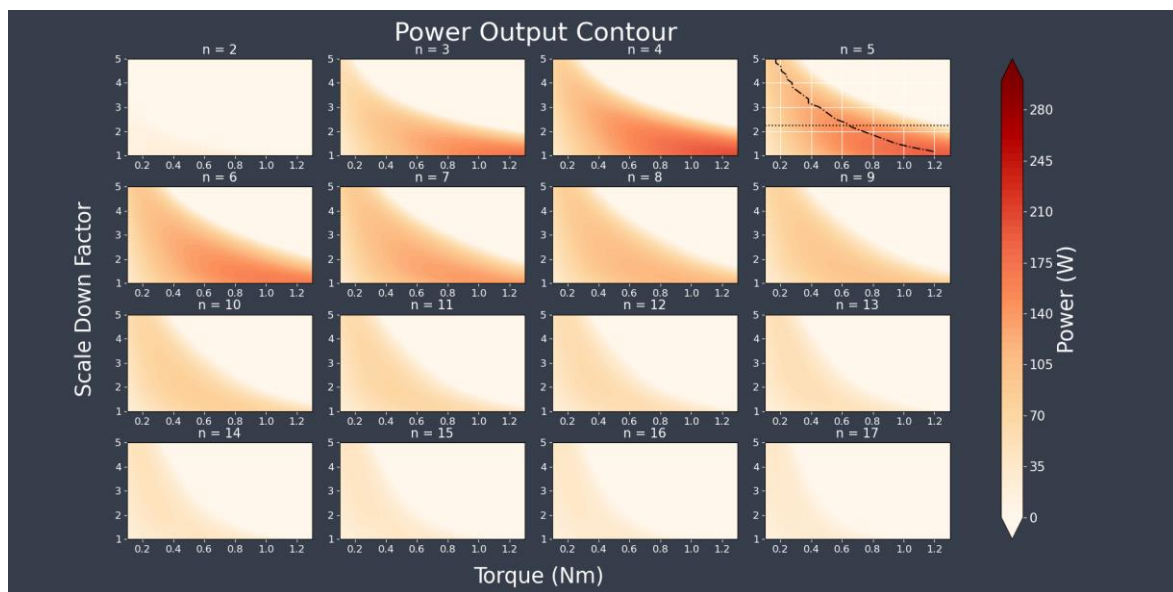

Figure 6 Power Contour at varying torque, scale down factor and disc numbers.

Figure 7 shows the Torque vs RPM plots for different surface microstructure profile, n and 4 mass flow rates, $\dot{m}$ instances. It is evident that all lines have decreasing trend with higher RPM settings. This is mainly due to lower relative velocity difference between the fluid and that of the rotating discs, leading to lower drag force and thus, lower overall torque.

Furthermore, the gradient steepness also seems to decrease with higher n value. On top of that, there are also instances where the lines converged at a certain RPM such as that in the top left corner diagram. A possible explanation to this occurrence is the different near wall velocity gradient for these profiles, where higher n proved greater potential for shear extraction and thus, able to maintain this property more efficiently at increasing RPM.

The convergence property on the other hand implies that lower n values may in fact, apply higher torque to the discs below a certain RPM. This is mainly attributed by the distance relative path lines traversed by the fluid at different profiles as shown in **Figure 8**.
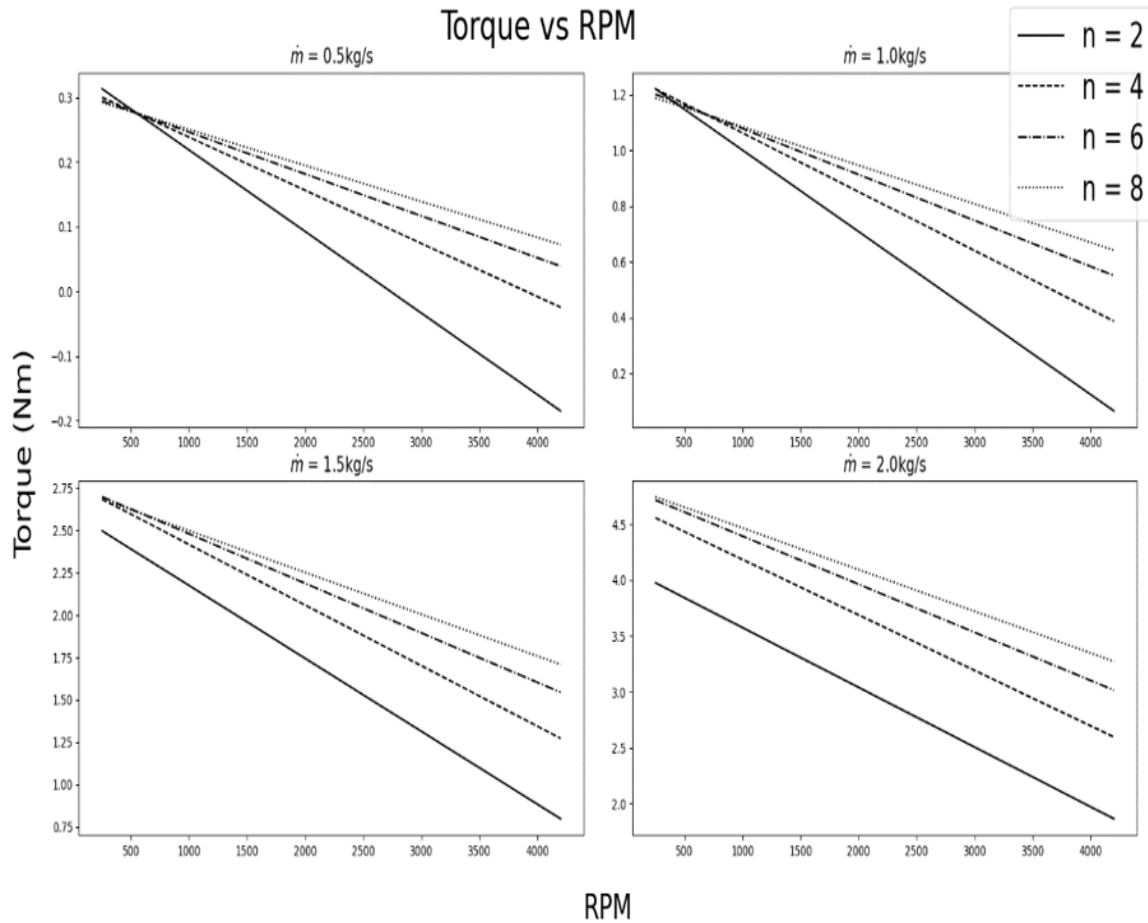

Figure 7 Torque vs RPM plots at different mass flow rate settings.

Based on **Figure 8**, at RPM = 200, the pathlines observed for $n = 2$ and $n = 8$ are very distinct, where the total circumferential distance travelled by fluid at $n = 2$ appears to be farther. This result is not out of the blue since higher n indicates higher shear extraction, which in turns leads the flow to taper off faster into radial dominant structure. Although this feature is highly sought after, but at low RPM the torque integral will end up smaller than that of longer distance, gradual decrease flow as provided by lower n flow. In the effort of attaining higher torque value, n profile and the intersecting RPM have to be equally considered for such applications.

Also according to **Figure 8**, regardless of the mass flow rates and n values, all lines clearly exhibit linear property as RPM varies. Although this may seem counterintuitive given the non-linearity of Equation 1, it is vital to note that all the factors within the ODE are not affected by RPM as such, differences in the final solution are only due to the inlet boundary condition, $\widehat{W}_0$. According to the torque formula in **Equation 26 (Group report)**, the denominator term, U_0 (RPM dependent) from $\widehat{W}$ will cancel out with the constant term outside the integral. Ultimately, this leaves the expression with just $\bar{v}_\theta = v_\theta - \omega r$, that consists a negative RPM dependent term and thus, explaining the linear profile above.
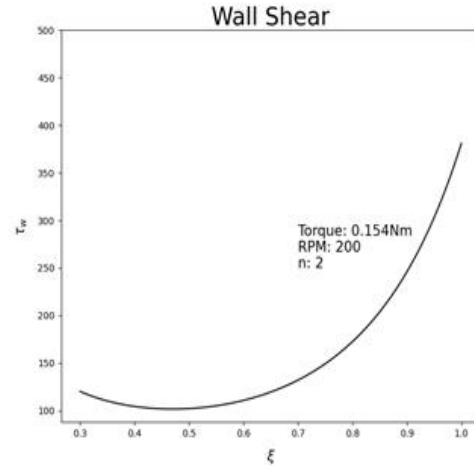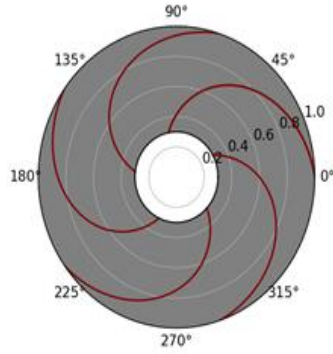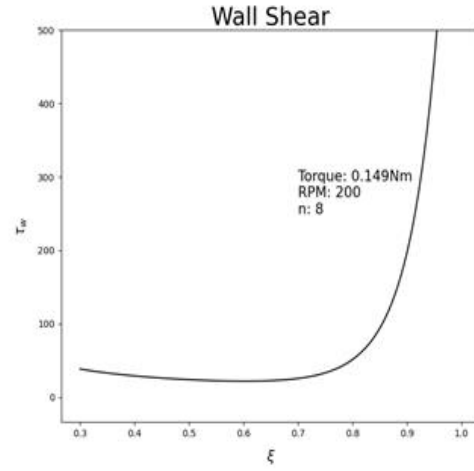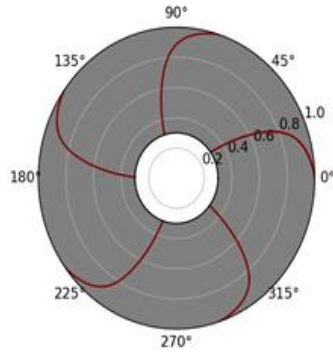
Figure 8 Relative pathlines and shear profile for n equal (a) 2 and (b) 8.

Maximum Power Formulation

Having the linear relation in place, we can then fit in the following equation to the plots:

$$T = m(RPM) + c$$

where *m* and *c* are the gradients and y-intercept which can be determined using any two simulation points in the above incidents. The maximum power can finally be derived using the steps as shown below:

$$P_{total} = T * RPM$$

$$\frac{d(P_{total})}{dRPM} = 2m(RPM) + c = 0$$

$$RPM = -\frac{c}{2m}$$

$$P_{max} = -\frac{c^2}{4m}$$

where P_{max} is the maximum attainable total power output.

2.4 CFD and Analytical Validation

After the model production, I also took part in CFD analysis, especially so for post processing to extract and cross validate results with that of the analytical model. In this phase, I worked alongside our team's CFD lead, Shawn Navarednam and Logistic Officer, Nicholas Khor for data comparison. My main task in this is to process raw CFD data extracted in xy format, then parse them over to python code and followed by validation plots. Most of these processes end with me sorting the data and plotting it in Python using matplotlib. In the occasional instances where further processing is required, I would then use **Pandas** library, converting and storing data in excel sheets before resending them back to Shawn.

One of the core results that I have extracted was tabulated in **Table 2**, showing the power output value comparison between CFD and that of analytical set after processing.

Table 2 Power output for different numerical models.

Model	Power Output (W)
Analytical	148
CFD (10 axial cells per disc)	206
CFD (20 axial cells per disc)	216

Seeing the huge disparity between the analytical and CFD counterpart, we then further investigate upon this matter by assessing the fundamental velocity components, in which the results were plotted as shown in **Figure 9**.

As observed from Figure 9, it is rather apparent that the CFD profile did not match the analytical dataset (black lines) regardless of what n modifying values it holds. However, it is worth noting that on average, the flow near the wall shows close resemblance to characteristics of $n = 8$ as compared to the rest ($n = 2, 4, 6$). One reasoning to this is the growing turbulence effects due to increasing velocity as it converged to the middle outlet of the discs. Based on mass conservation, the flow's radial velocity should follow an inverse profile that is dependent on the radial position. Basically, with an inlet radial component of ~2.8 m/s, the outlet radial component will be magnified to as large as ~9 m/s. This will likely cause turbulence effect to occur which also explains why the profile continues to flatten out as ξ decreases (in comparison to ξ = 0.924). Correspondingly, the CFD's near wall velocity gradient will yield higher value and thus, providing greater shear output. The inference here is also supported by the fact that the CFD solver could not converge properly when using a laminar solver, but did so effectively while using $k - \varepsilon$ modelling. In essence, the laminar assumption in the analytical set may not hold true for our turbine design as such, an improved model would have to be implemented.

Aside from that, another critical observation gotten here was the abrupt profile transition from ξ = 0.993 to ξ = 0.924. This is very likely due to entrance effects which were never accounted for in the analytical model, further contributing to the distinction obtained in **Table 2**. From these obtained conclusions, I was then convinced that the model though widely implemented, does not encompass all of the necessary flow physics as such, causing wide deviations in the performance values. Adjustments have to be inserted to account for the flow state transitions and

entrance effects for better results mapping as well as truly leveraging the use of numerical modelling for such applications.
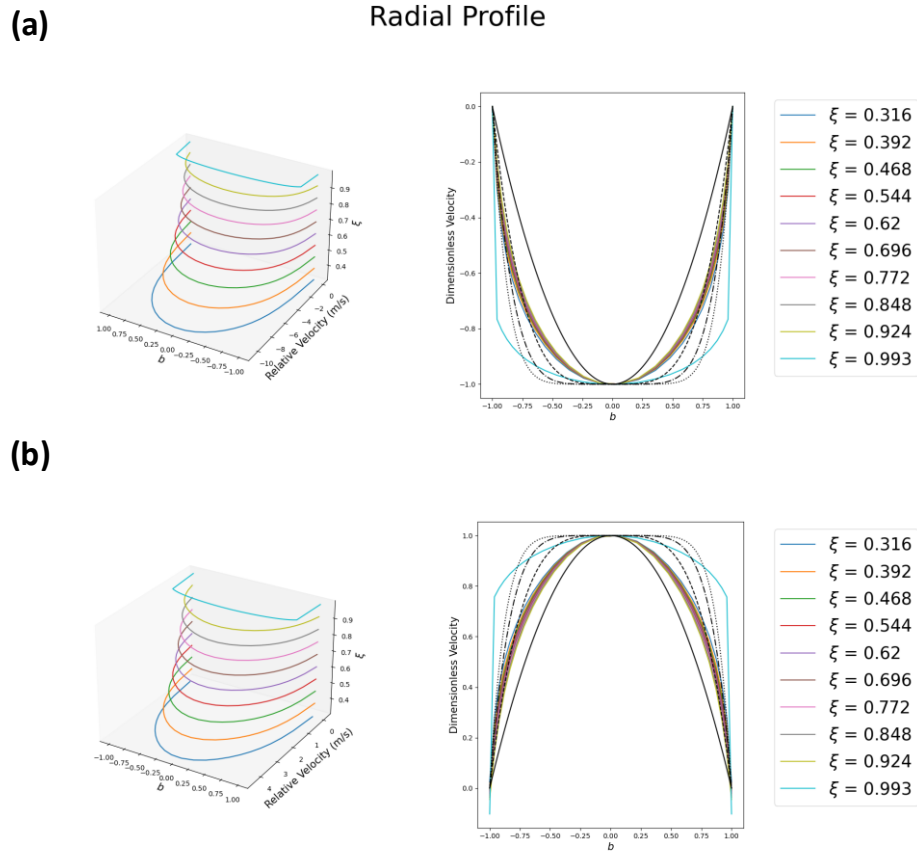
(a)

Radial Profile

(b)

Figure 9 CFD flow velocity profiles at different radial instances.

2.5 Embedded programming

For this project, I also contributed in writing out the Arduino test code for sensor data extraction. I also supported in searching for Arduino compatible sensors (flow meter, pressure & infrared sensors) as well as the electronic schematic diagram.

With the objective of extracting sensors' data seamlessly, I investigated the example setups provided in the user manuals, understanding the varying reading methods for each sensor. The flow meter and IR sensor function via pulse frequency operation, whereas the pressure data can be directly obtained through Analog read. Essentially, this will affect the extraction process for each component and hence, a universal sampling rate (1s) was included to sync up the results within an acceptable accuracy margin.

Although the code and testing samples were ready to be executed, unfortunately due to lockdown restrictions, our team then proceed on with a fully numerical project and thus, abandoning manufacturing and the need for experimental data evaluations.

2.6 Report Writing

Having done all of the numerical work, I was put in charge to write up this section of the group report (**Section 4**), properly documenting the entire methodology alongside key analytical results. Furthermore, I also help out in proof-reading the entire report, tidying up and ensuring the content falls in their appropriate places.

3 Key achievements

- Literature Reviews on numerical modelling and their applications in tesla turbine.
- Codebase formulation for numerical simulation purposes.
- Turbine design optimisation via simulated results.
- Further performance results for analytical studies.
- CFD results processing & validation with analytical sets.
- Results explanations based on literature and fluid mechanics understanding.
- Report write-up.

4 Critical review

The table below lists out my personal review of this project on the overall scheme.

Table 3 Project critical review.

Aspects	Comments
Innovation	Implementation of a novel volute design, making the turbine versatile and applicable in a wide range of river settings for rural electrification. Simplified testbench and assembly design that accounted for performance and costing.
Process	The project plan was not clearly outlined at the beginning of the process, despite having done comprehensive literature review and consultations. The team has severely underestimated the manufacturing process and things associated with practical setups, which was a huge inhibiting factor in the overall progress. On top of that, the limited manufacturing period due to lockdown further add on to this worry, and eventually led the project's focus into an entirely numerical project. Fortunately, the progress on the numerical and CAD design front has never faltered, which helped to patch things up and put us right back on track.
Communication	Due to the project being fully numerical, most of the work was presented in graphical manner for better explanations to both technical and non-technical audience. The video and slide presentations were adjusted especially for non-technical audiences due to the short time span allowed. However, thorough technical explanations were included inside the report to give better insights on the full design process as well as the final results attained.

References

[1] W. Rice, "An Analytical and Experimental Investigation of Multiple-Disk Turbines," *J. Eng. Power*, pp. 1–8, 1965.

[2] S. Sengupta and A. Guha, "A theory of Tesla disc turbines," *Proc. Inst. Mech. Eng. Part A J. Power Energy*, vol. 226, no. 5, pp. 650–663, 2012, doi: 10.1177/0957650912446402.

[3] V. D. Romanin, "Theory and Performance of Tesla Turbines," p. 98, 2012.

[4] V. G. Krishnan, V. Romanin, V. P. Carey, and M. M. Maharbiz, "Design and scaling of microscale Tesla turbines," *J. Micromechanics Microengineering*, vol. 23, no. 12, 2013, doi: 10.1088/0960-1317/23/12/125001.

[5] J. A. Keep and I. J. Jahn, "Design method and performance comparison of plenum and volute delivery systems for radial inflow turbines," *Proc. 20th Australas. Fluid Mech. Conf. AFMC 2016*, no. December, 2016.